Suppprting Information

A New Co(II) Thiocyanato Coordination Polymer with 4-(3-Phenyl-propyl)pyridine: Influence of the Co-Ligand on the Magnetic Properties

Julia Werner, Michał Rams, Zbigniew Tomkowicz, and Christian Näther

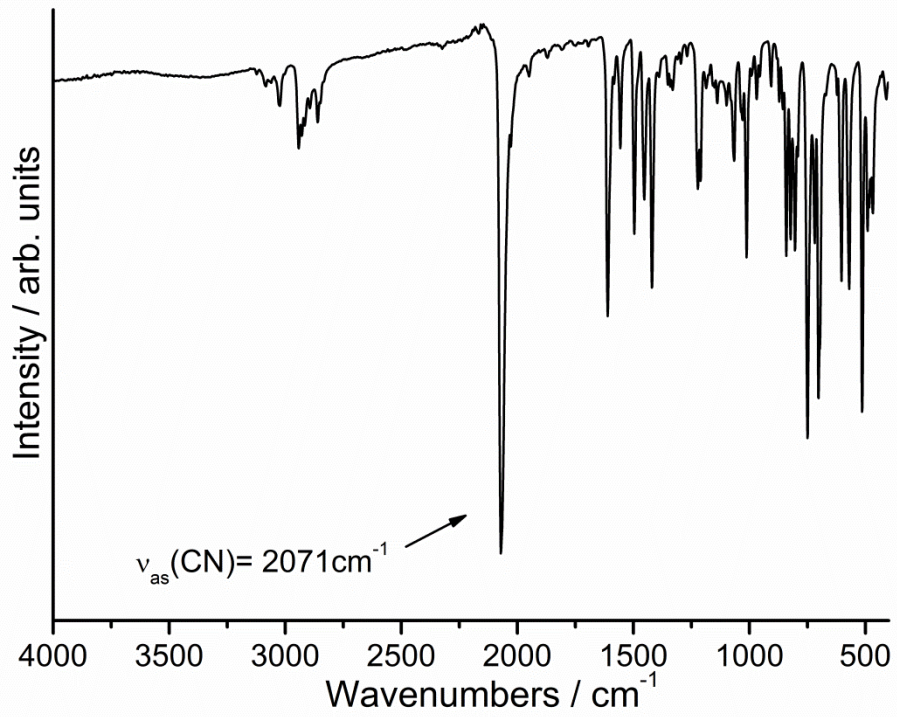

Figure S1. IR spectra of compound **1**.

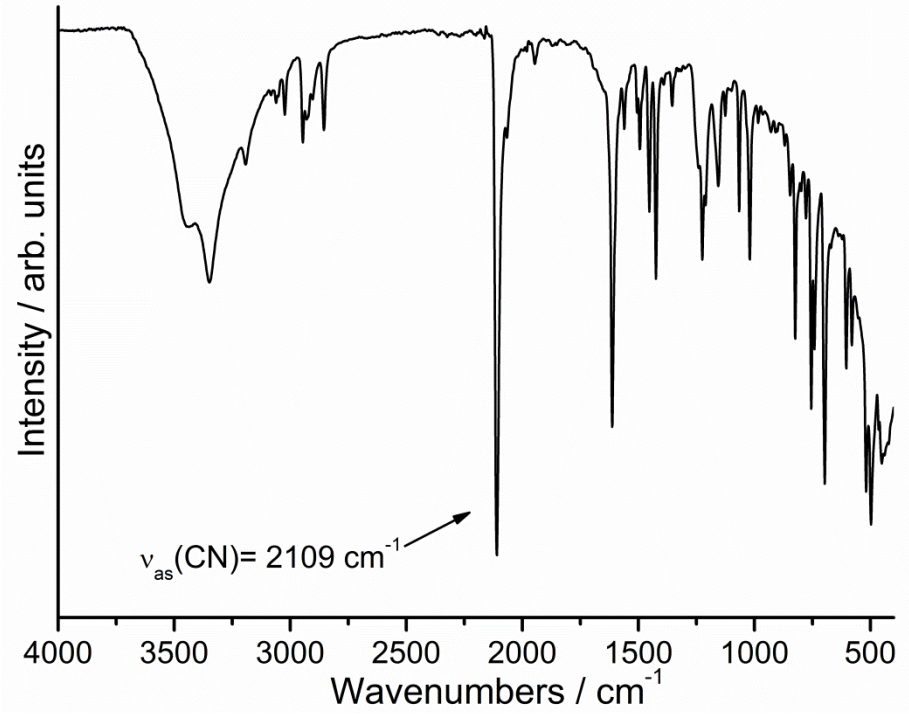

Figure S2. IR spectra of compound **2**.

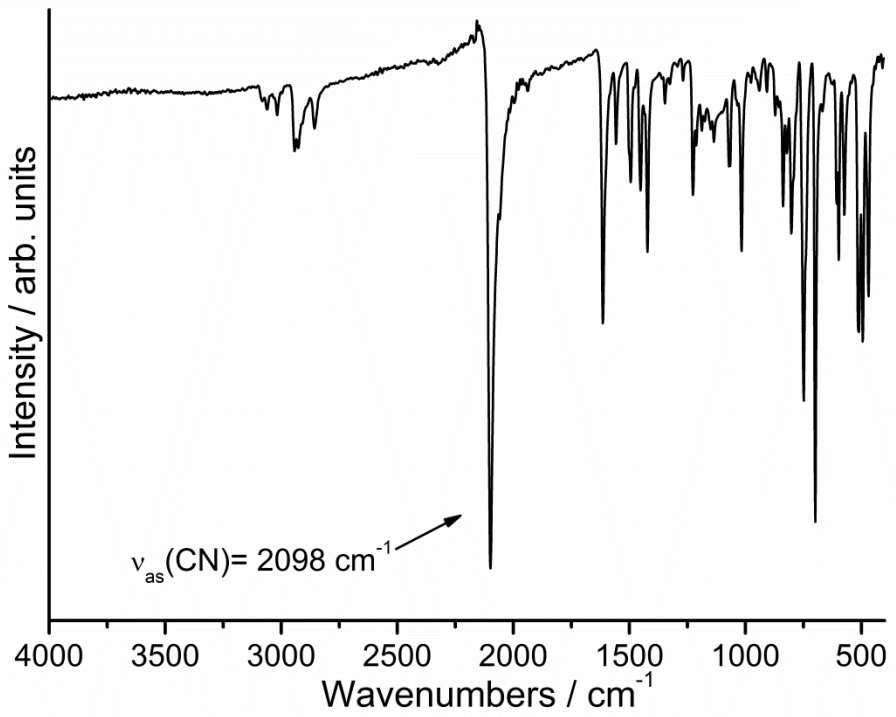

Figure S3. IR spectra of compound **3**.

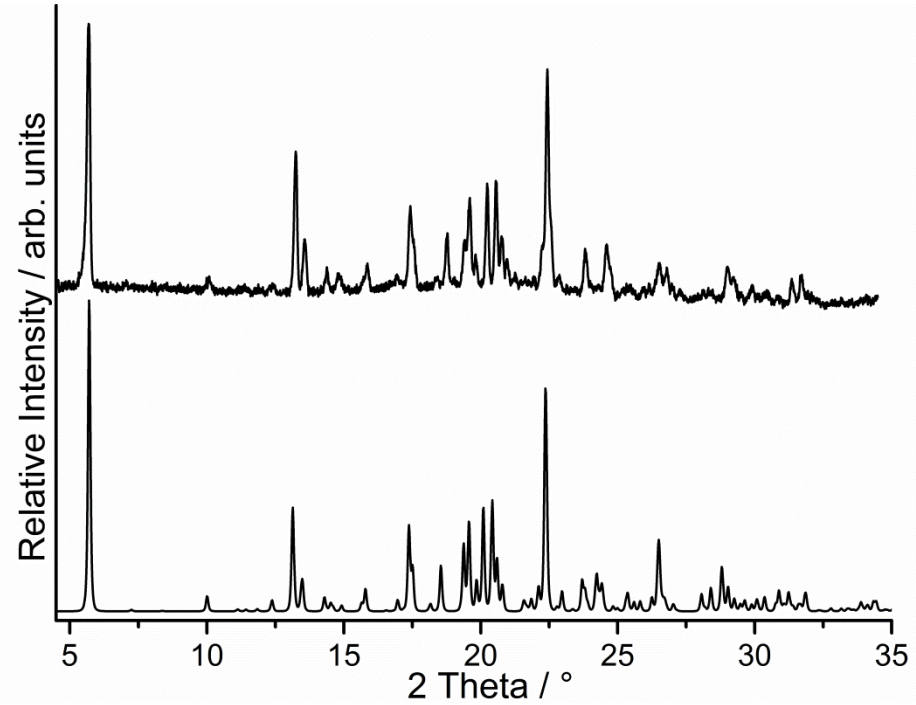

Figure S4. Experimental (top) X-ray powder pattern of compound **2** measured in transmission geometry and calculated X-ray powder pattern of $Mn(NCS)_2$(4-(3-Phenylpropyl)pyridine)$_2(H_2O)_2$ retrieved from literature (bottom).

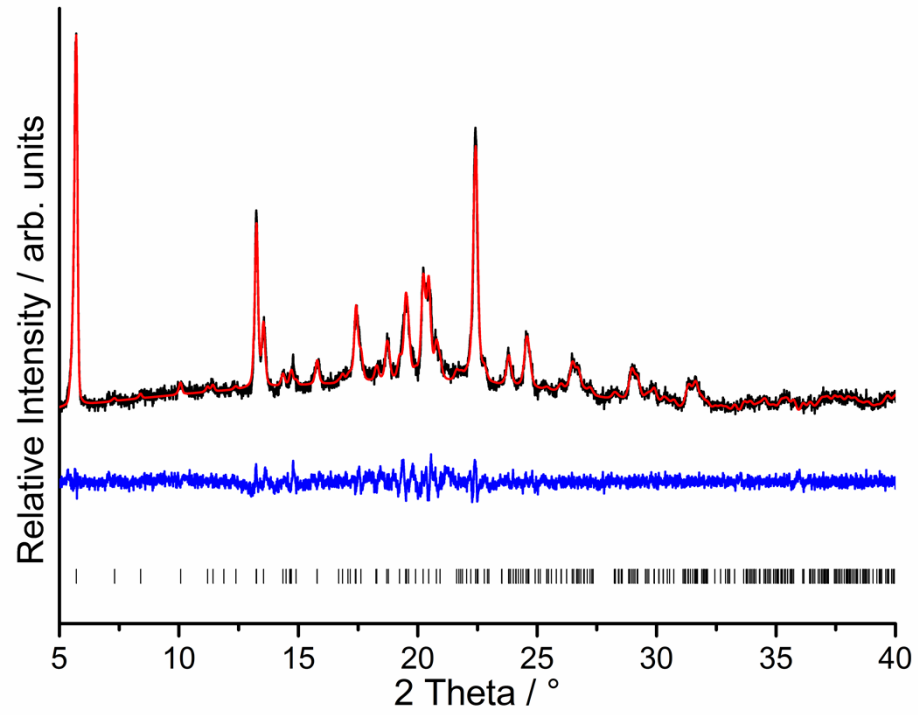

Figure S5. Pawley fit of a pattern of compound **2** measured in transmission geometry.

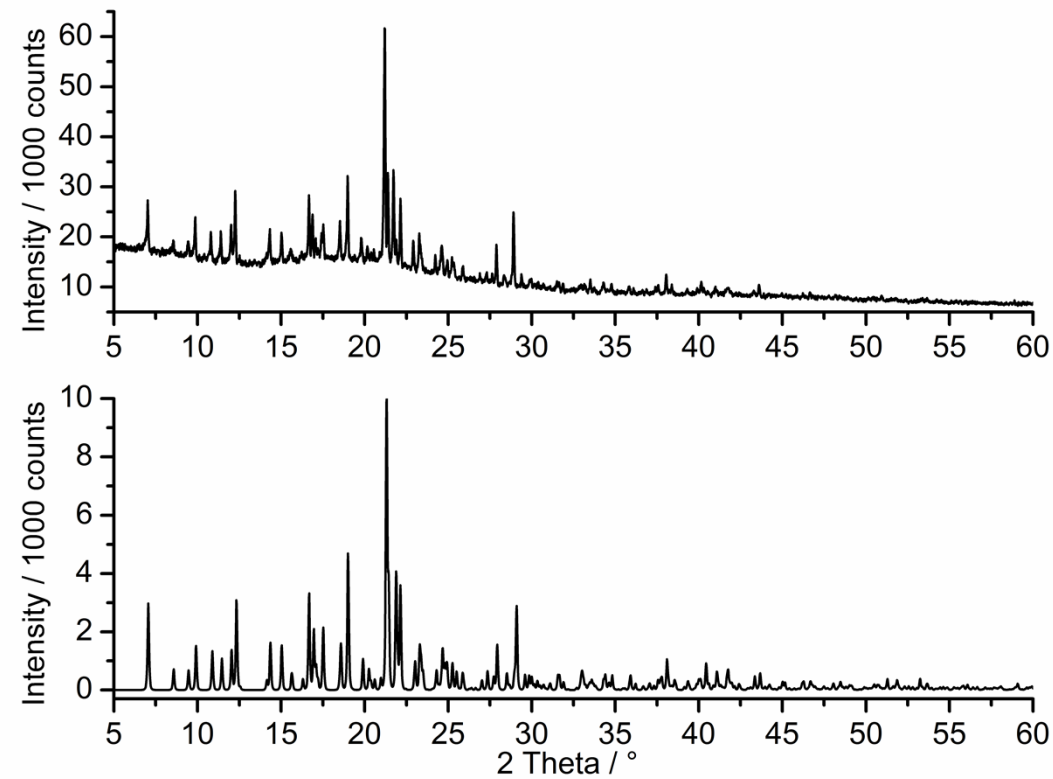

Figure S6. Experimental (top) and calculated (bottom) X-ray powder pattern of compound **1** measured in refelction geometry.

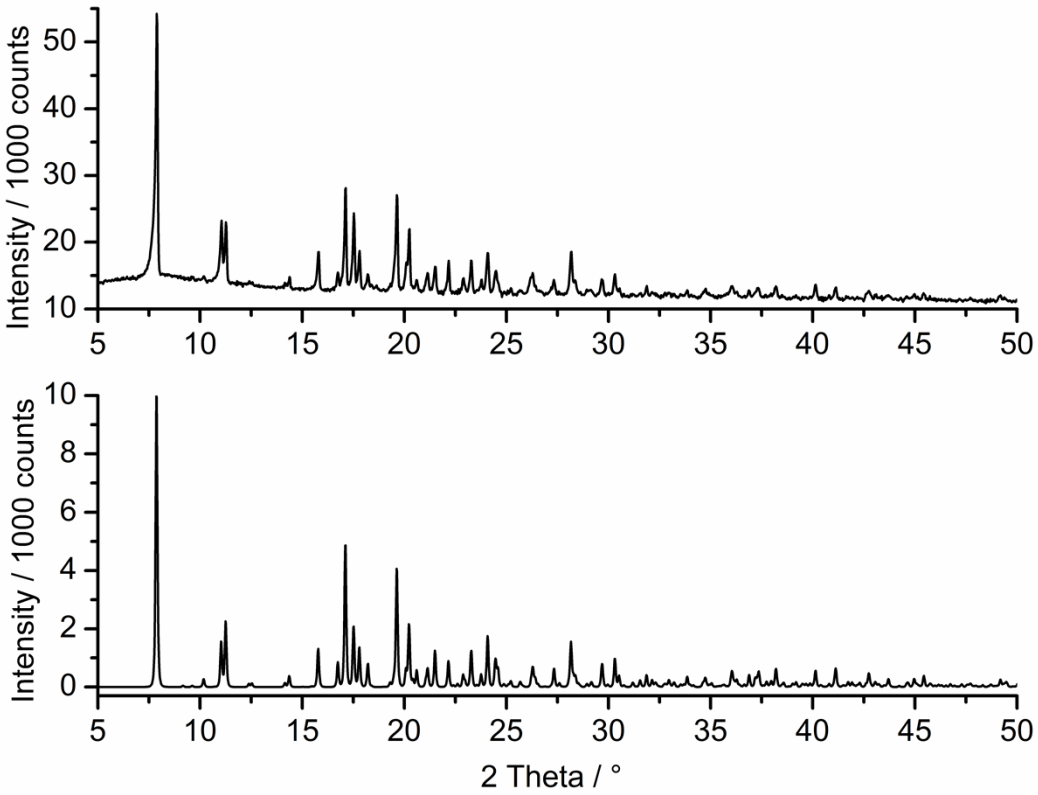

Figure S7. Experimental (top) and calculated (bottom) X-ray powder pattern of compound **3** measured in reflection geometry.

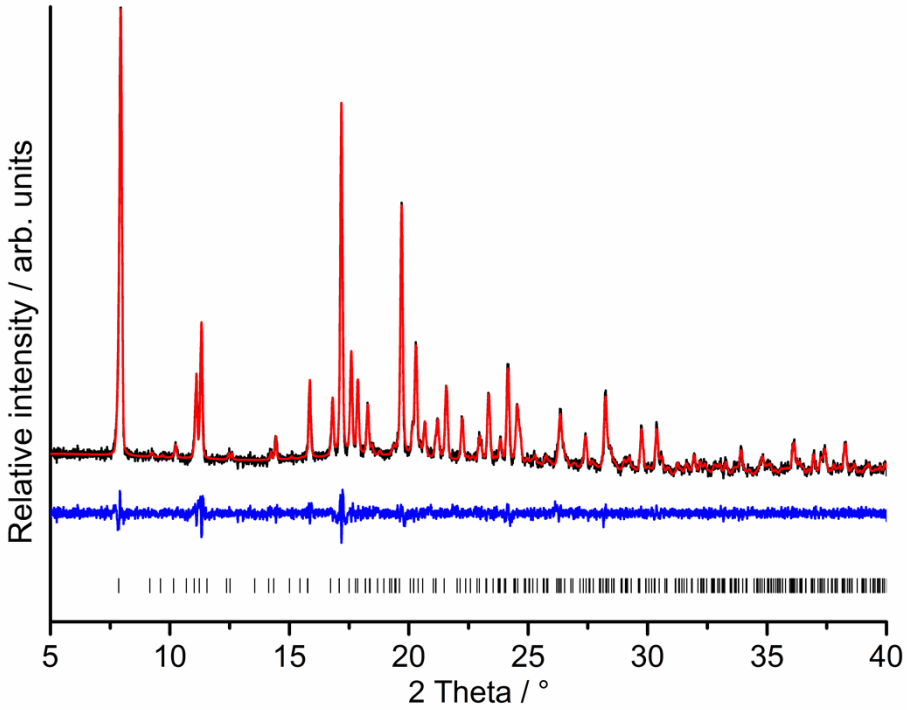

Figure S8. Pawley fit of a pattern of compound **3** measured in reflection geometry.

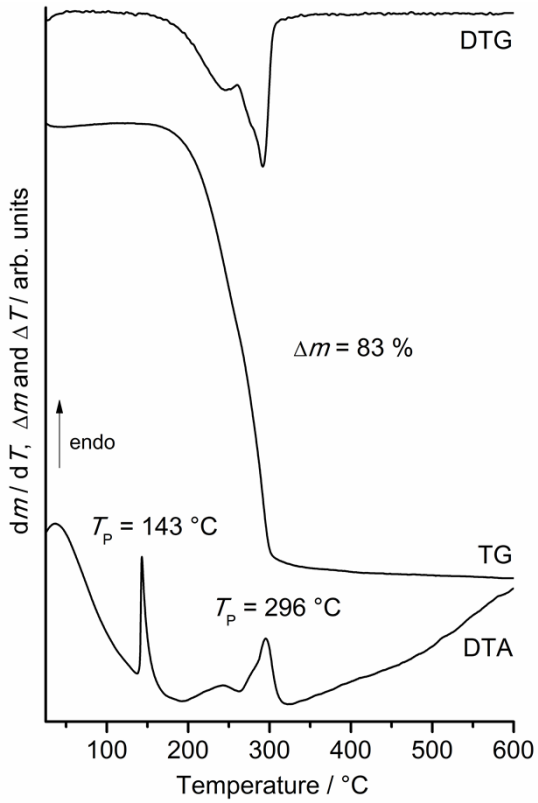

Figure S9. DTA-, TG- and DTG-curve of compound **1**. Heating rate = 4 °C/min.

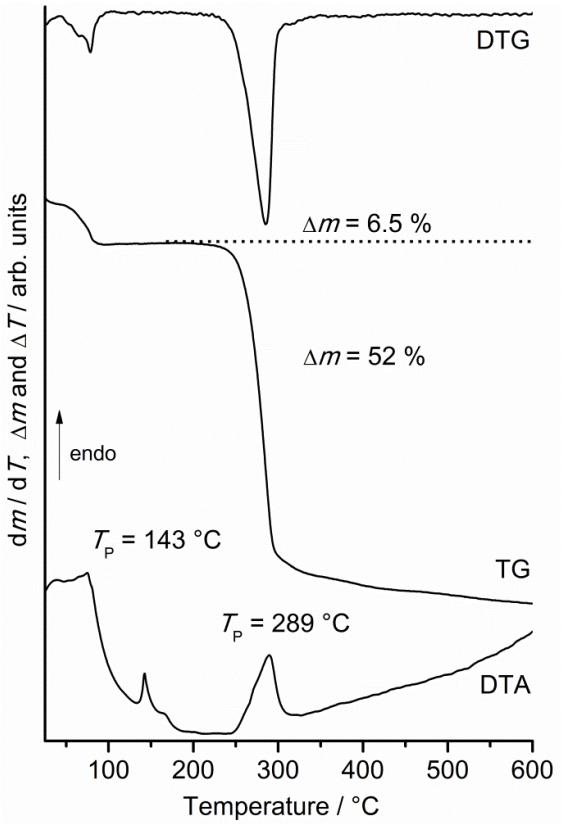

Figure S10. DTA-, TG- and DTG-curve of compound **2**. Heating rate = 4 °C/min.

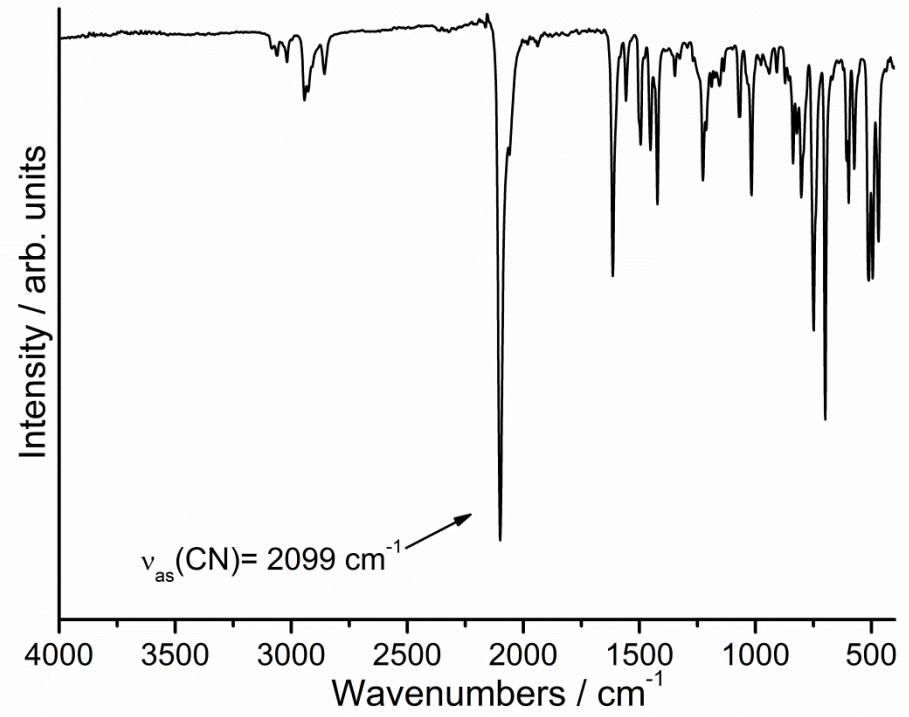

Figure S11. IR spectra of the residue of obtained by thermal decomposition of **2**.

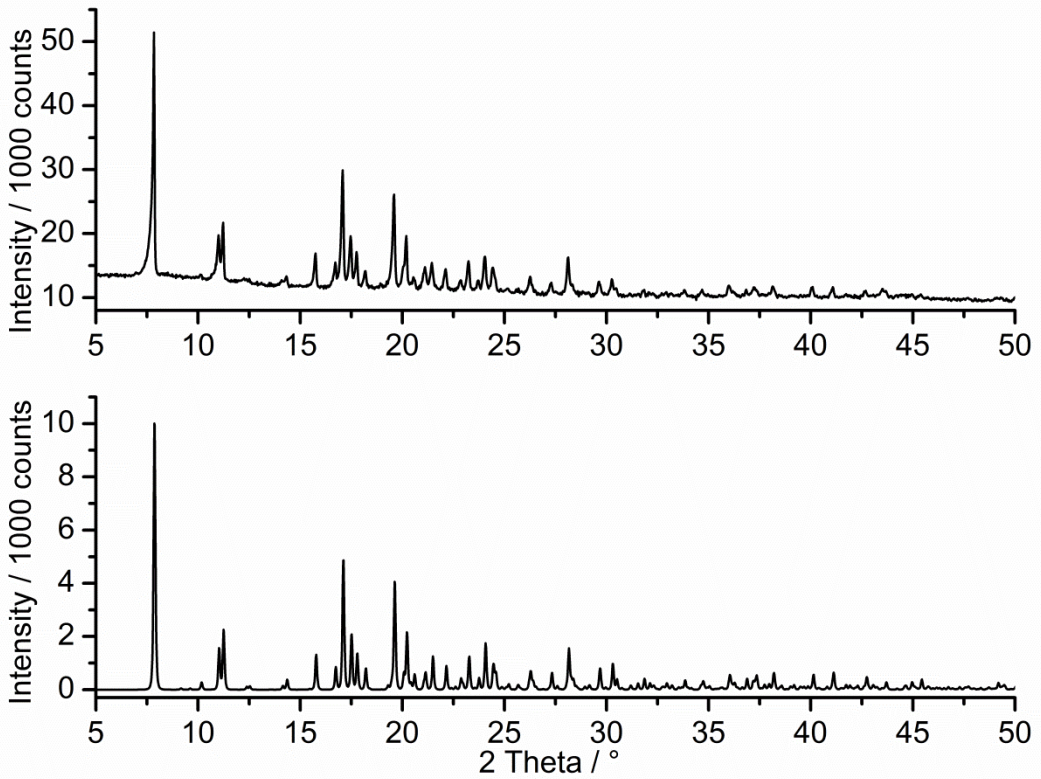

Figure S12. Experimental X-ray powder pattern of the residue obtained by thermal decomposition of **2** (top) and calculated pattern for **3** (bottom).

Table S1. Selected bond lengths (Å) and angles (°) for **1**.

Co(1)-N(1)	2.0809(16)	Co(1)-N(31)	2.1922(14)
Co(1)-N(11)	2.2466(15)		
N(1A)-Co(1)-N(1)	180.000(1)	N(1)-Co(1)-N(11)	88.36(6)
N(1)-Co(1)-N(31A)	89.16(6)	N(31)-Co(1)-N(11A)	88.12(5)
N(1)-Co(1)-N(31)	90.84(6)	N(31)-Co(1)-N(11)	91.88(5)
N(1)-Co(1)-N(11A)	91.64(6)		

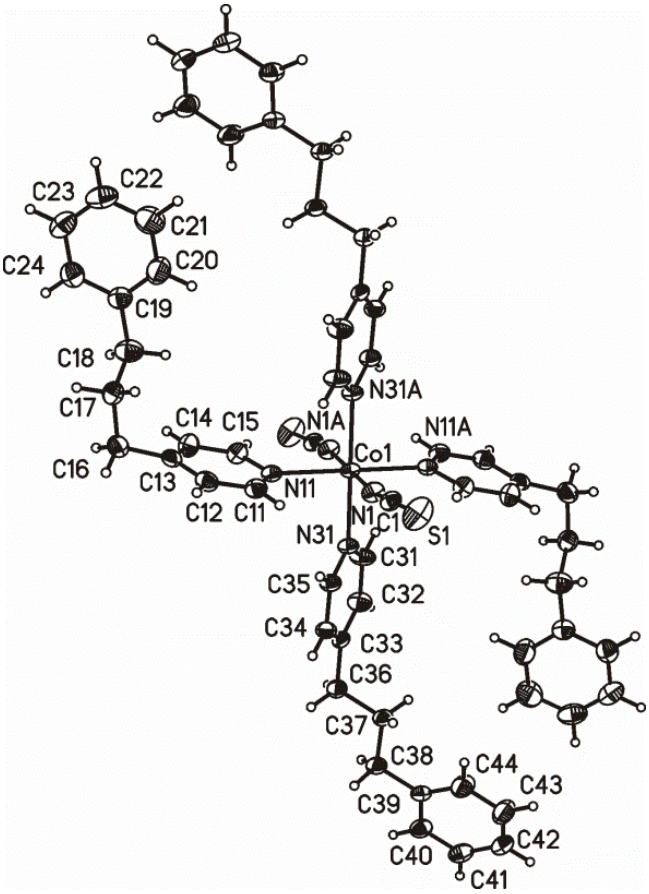

Figure S13. ORTEP plot of **1** with labelling and displacement ellipsoids drawn at the 50 % probability level. Symmetry transformation used to generate equivalent atoms: A: -x+1,-y+1,-z+1.

Table S2. Selected bond lengths (Å) and angles (°) for **3**.

Co(1)-N(1)	2.077(4)	Co(2)-N(2)	2.055(4)
Co(1)-N(11)	2.161(4)	Co(2)-N(31)	2.169(5)
Co(1)-S(2)	2.5801(13)	Co(2)-S(1)	2.6232(14)
N(1)-Co(1)-N(1A)	180.0(2)	N(31B)-Co(2)-N(31)	180.0(2)
N(1)-Co(1)-N(11)	89.69(16)	N(2)-Co(2)-N(31)	90.13(18)
N(1)-Co(1)-N(11A)	90.31(16)	N(2)-Co(2)-N(31B)	89.87(18)
N(1)-Co(1)-S(2)	93.46(12)	N(2)-Co(2)-S(1)	93.69(12)
N(1)-Co(1)-S(2A)	86.54(12)	N(2)-Co(2)-S(1B)	86.31(12)
N(11)-Co(1)-S(2)	92.03(12)	N(31)-Co(2)-S(1)	91.46(12)
N(11)-Co(1)-S(2A)	87.97(12)	N(31)-Co(2)-S(1B)	88.54(12)

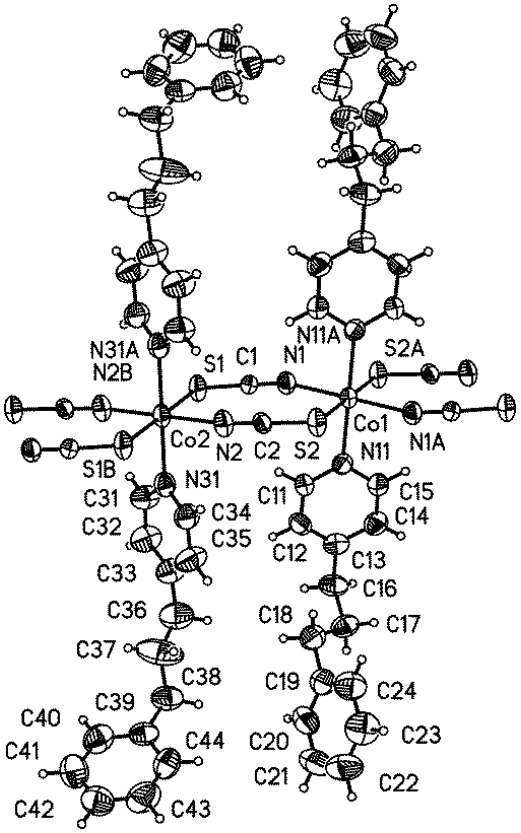

Figure S14. ORTEP plot of **3** with labelling and displacement ellipsoids drawn at the 50 % probability level. Symmetry transformation used to generate equivalent atoms: A: -x,-y+1,-z, B: -x+1,-y+1,-z.

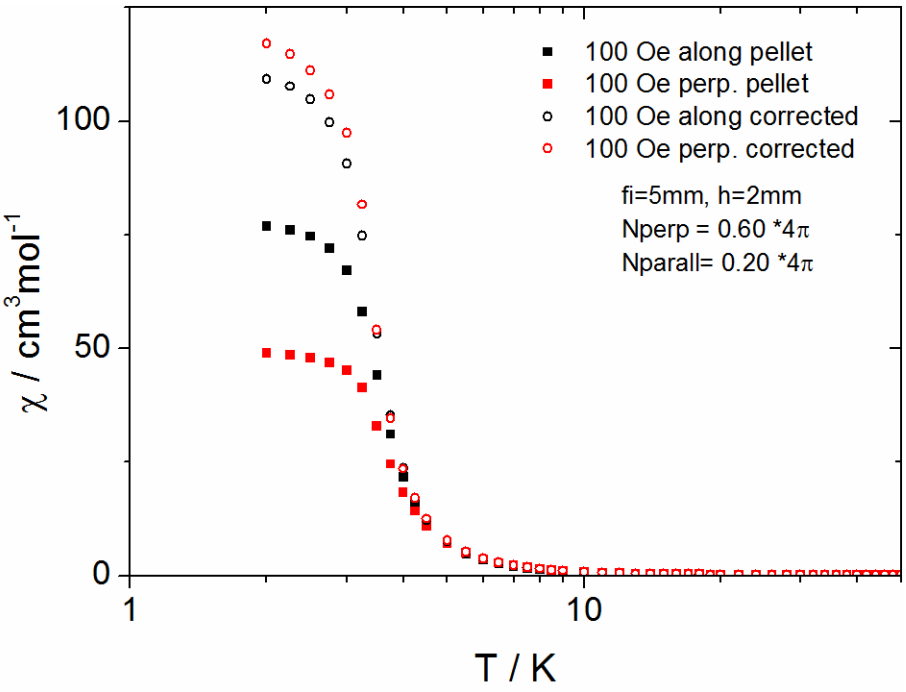

Fig. S15. The influence of demagnetization on the measured low temperature susceptibility of compound **3**. The two curves were measured using the same pellet sample, once oriented perpendicular to the field (red), and once with the flat parallel to the field (black). The open symbols denote the values corrected for the demagnetization effect. The demagnetization factors used in the two cases fulfill relation $N_{\perp} + 2N_{\parallel} = 4\pi$.

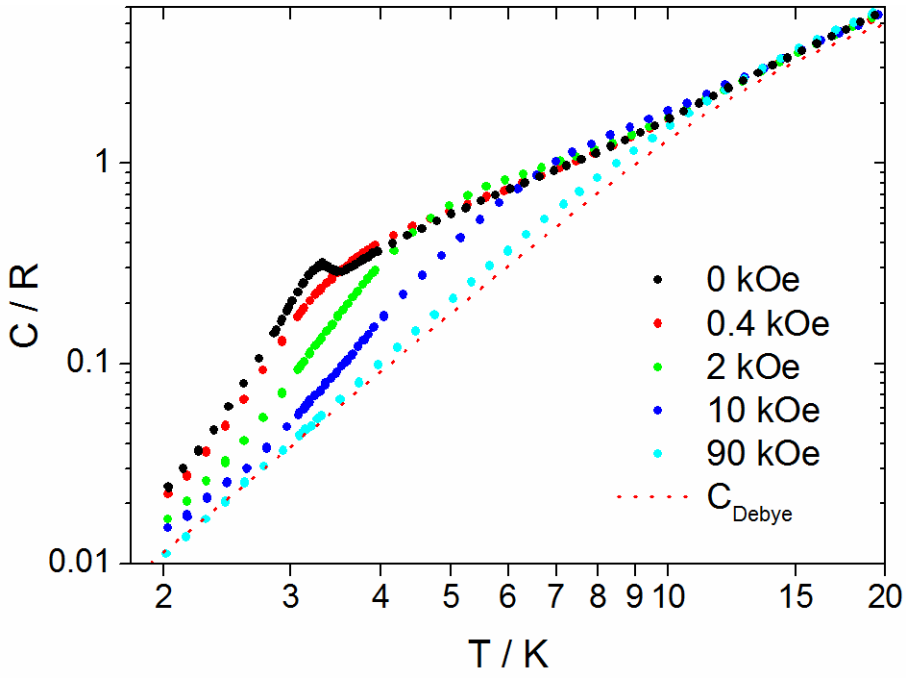

Fig. S16. Specific heat of compound **3** measured at different applied fields, using a powder sample. The dotted line represents the phonon contribution C_{Debye} to the specific heat, fitted as described in the main text. C_{Debye} is close to the experimental points measured at 90 kOe. This is expected, because high magnetic field aligns magnetic moments and the entropy change related to spins is shifted to higher temperatures. In the case of **3**, even a higher field would be necessary to obtain precisely the phonon contribution directly from the specific heat measurements. This is due to the high anisotropy of Co^{II} ions and random orientations of crystallites in the powder sample. For this reason we have chosen to fit the phonon contribution together with the magnetic contribution, and not to assume that 90 kOe data represents the phonon contribution only. The field of 0.4 kOe is enough to conceal the peak observed at zero magnetic field. The internal field is much smaller due to the demagnetization field. The demagnetization factor is close to $N = 4\pi$ for the thin, flat sample oriented perpendicular to the external field. The demagnetization field $H_{demag} = -NM/V$, where M/V is the magnetic moment per volume, is strongly dependent on temperature, due to strong $M(T)$ dependence. At T_c =3.3 K and below we estimate H_{demag} = -0.35(5) kOe basing on the magnetic measurements. At 0.4 kOe the $M(H)$ curve (measured for such a sample geometry) is already saturated above 1.5μ_B, which corresponds to lack of the peak in specific heat, already at 0.4 kOe.

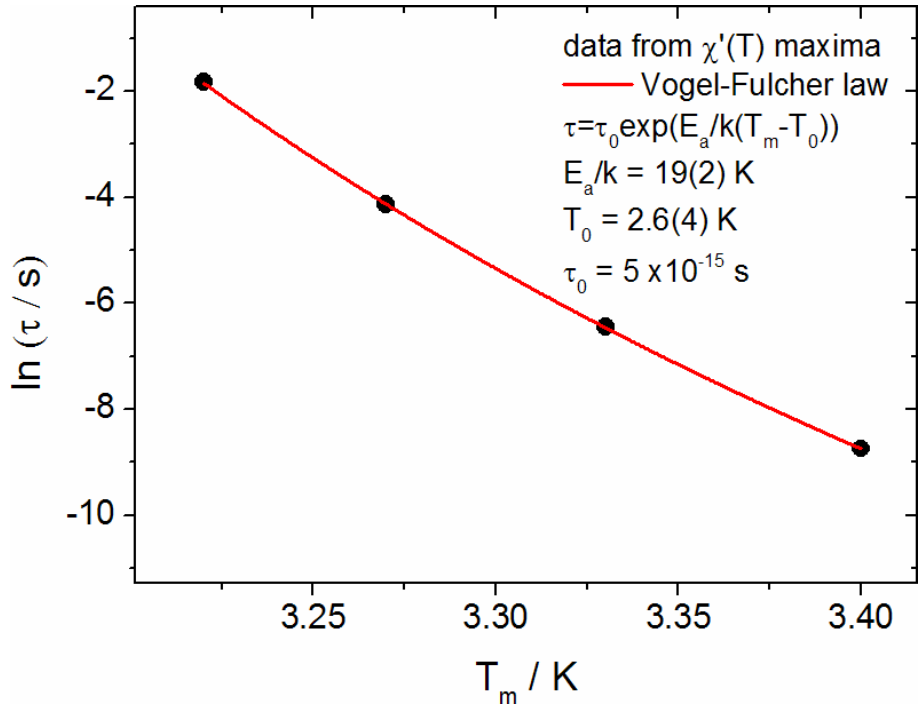

Fig. S17. Analysis of the temperature dependence of the relaxation time for **3.** T_m is the position of the $\chi'(T)$ maximum from ac measurement made using different frequency f. The relaxation time $\tau = 1/(2\pi f)$. The fit using the Vogel-Fulcher law is shown by solid line.

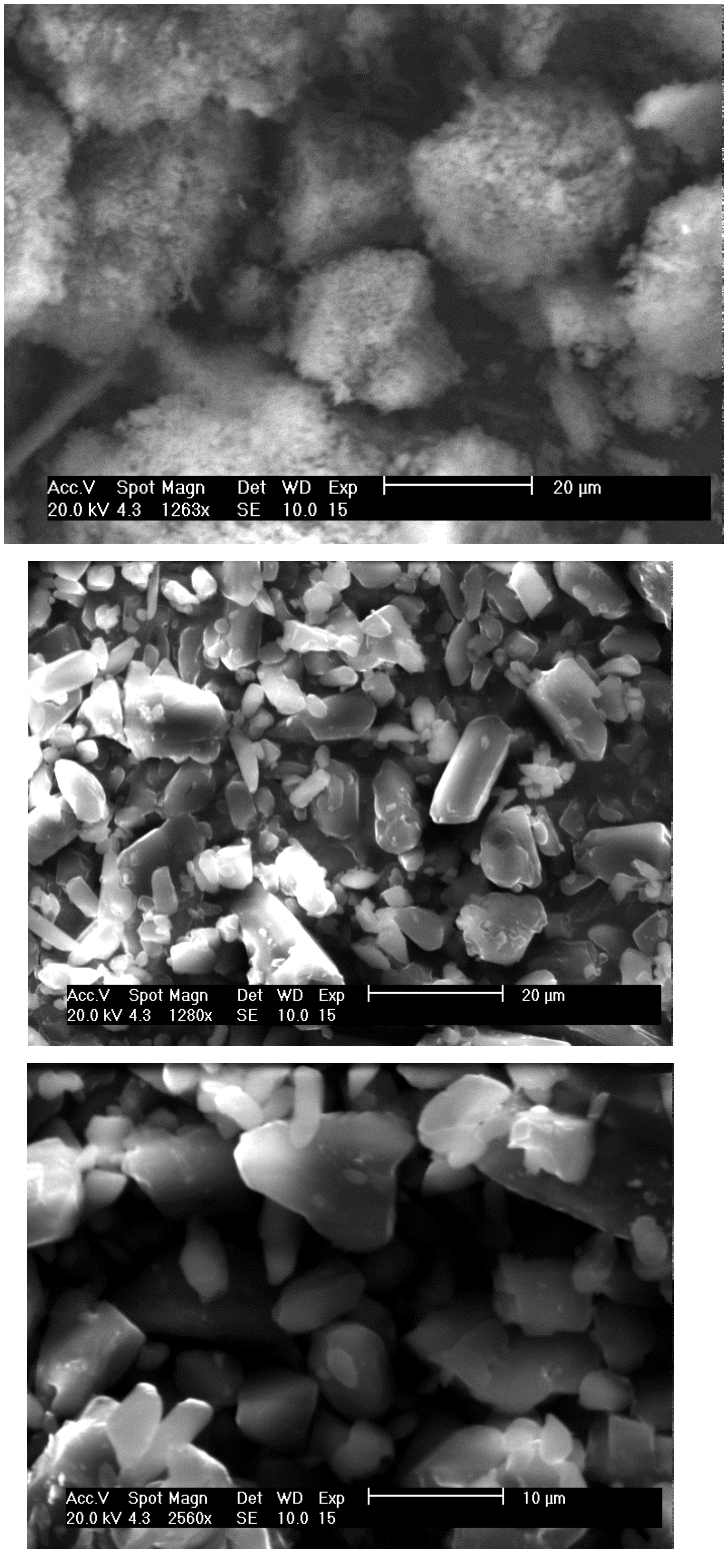

Fig. S18. SEM images of compound **3** obtained after thermal annealing (top) and obtained by synthesis at RT (mid and bottom).